ELSEVIER

Biophysical Chemistry 100 (2003) 577–591

Biophysical Chemistry

www.elsevier.com/locate/bpc

Prospects of electron cryotomography to visualize macromolecular complexes inside cellular compartments: implications of crowding☆

Kay Grünewald[a,b], Ohad Medalia[a], Ariane Gross[a], Alasdair C. Steven[b], Wolfgang Baumeister[a,*]

[a]*Department of Structural Biology, Max Planck Institute of Biochemistry, Am Klopferspitz 18a, D-82152 Martinsried, Germany*
[b]*Laboratory of Structural Biology, National Institute of Arthritis and Musculoskeletal and Skin Diseases, National Institutes of Health, 50 South Drive MSC 8025, Bethesda, MD 20892-8025, USA*

Received 23 March 2002; accepted 7 June 2002

Abstract

Electron cryotomography has unique potential for three-dimensional visualization of macromolecular complexes at work in their natural environment. This approach is based on reconstructing three-dimensional volumes from tilt series of electron micrographs of cells preserved in their native states by vitrification. Resolutions of 5–8 nm have already been achieved and the prospects for further improvement are good. Since many intracellular activities are conducted by complexes in the megadalton range with dimensions of 20–50 nm, current resolutions should suffice to identify many of them in tomograms. However, residual noise and the dense packing of cellular constituents hamper interpretation. Recently, tomographic data have been collected on vitrified eukaryotic cells (Medalia et al., Science (2002) in press). Their cytoplasm was found to be markedly less crowded than in the prokaryotes previously studied, in accord with differences in crowding between prokaryotic and eukaryotic cells documented by other (indirect) biophysical methods. The implications of this observation are twofold. First, complexes should be more easily identifiable in tomograms of eukaryotic cytoplasm. This applies both to recognizing known complexes and characterizing novel complexes. An example of the latter—a 5-fold symmetric particle is—given. Second, electron cryotomography offers an incisive probe to examine crowding in different cellular compartments.

Keywords: Electron tomography; Macromolecular crowding; Eukaryote/prokaryote distinction; Vitrification

1. Introduction

Cryo-electron microscopy (cryo-EM) [1–4] encompasses the various techniques of studying biological specimens preserved for observation by rapid freezing. Although the term formally includes methods in which the water is subsequent-

☆ This paper is dedicated to the memory of John T. Edsall in recognition of his fundamental contributions to the physical chemistry of proteins.

*Corresponding author. Tel.: +49-89-8578-2652; fax: +49-89-8578-2641.
E-mail address: baumeist@biochem.mpg.de (W. Baumeister).

0301-4622/03/$ - see front matter © 2002 Elsevier Science B.V. All rights reserved.
PII: S0301-4622(02)00307-1

ly removed and the specimen contrasted by metal shadowing (as in freeze-fracture) or staining (as in freeze substitution), it has increasingly come to refer to experiments in which the specimen is observed directly in ice, in the state in which it was immobilized by cryo-fixation [5]. If the freezing is rapid enough, vitrification is achieved, giving uniquely benign preservation of structure. Cryo-EM in this sense has developed in three major directions, namely, electron crystallography [6,7] (although in many such experiments, the specimens are still transferred to low temperature only after grid preparation in order to benefit from improved radiation-hardiness); 'single particle' analysis [8]; and tomography [9–11].

Electron tomography of ice-embedded specimens ('cryotomography') is maturing into a powerful tool with particular potential for studying specimens that are large and pleiomorphic, as has been demonstrated in studies of mitochondria [12] and of prokaryotic cells [13]. Although tomograms of pleiomorphic specimens cannot be directly enhanced by image averaging [14], they afford a basis on which three-dimensional representations of related specimens may be systematically segmented and compared. Another consequence of ineligibility for averaging is that it raises problems in defining empirical measures of the resolution achieved in tomograms, similar to the measures used in other branches of cryo-EM (15,16,17) which are based on detecting consistency of information between multiple copies of the same element-see-2.6. Nevertheless, there is good reason to believe that resolutions in the range of 5–8 nm have been achieved in cryotomography and further improvement as a result of technical innovations may be anticipated.

This inability to average means that it is not possible to suppress noise by this means, imposing a constraint that may ultimately limit the resolution of cellular tomograms to 3–4 nm (see section 2.6). However, resolutions of this order should still suffice to provide many incisive insights. In addition to observations from unaided tomography, one may anticipate a powerful symbiosis between 'single particle' analysis of isolated complexes and cryotomography of intracellular complexes that exploits the advantages of both approaches. In combination, they hold great promise for realizing a detailed understanding of structure-function relationships of macromolecular complexes in vitro and in situ. The prospects of this combined approach are enhanced in light of the growing realization that large macromolecular complexes are responsible for many fundamental biological processes [18–20].

In this review, we first summarize the basic principles of tomography, then discuss the various factors that limit the resolution and signal-to-noise ratio (SNR) of tomograms in practice. We show illustrative tomographic data of both prokaryotic and eukaryotic cells in the vitrified state, drawing attention to the markedly lower density of macromolecules in the eukaryotic cytoplasm. The consistency of this observation with data on molecular crowding previously ascertained by other biophysical techniques is then discussed. Finally, we consider future prospects with particular reference to macromolecular complexes. It is likely that cells house numerous complexes that have not been isolated and characterized in vitro for reasons of instability or paucity. We substantiate this proposal by showing a morphologically distinctive and hitherto unknown complex that has been detected in cryotomograms of *Dictyostelium* cells.

2. Principles of electron cryotomography

The basic idea of tomography is first to record a series of two-dimensional projection images of the object of interest as viewed from different directions, and then to synthesize these projections into a three-dimensional density map Fig. 1. To acquire the projections, the specimen holder is tilted incrementally around an axis perpendicular to the electron beam and an image is recorded at each position. To synthesize the density map, the projections are mutually aligned in a common frame of reference, and the map is then calculated—most commonly, by a 'weighted back-projection' algorithm [21].

2.1. Sample preparation by ice-embedding (vitrification)

Prerequisite for preservation of a cell and its contents in their native state is vitrification, i.e.

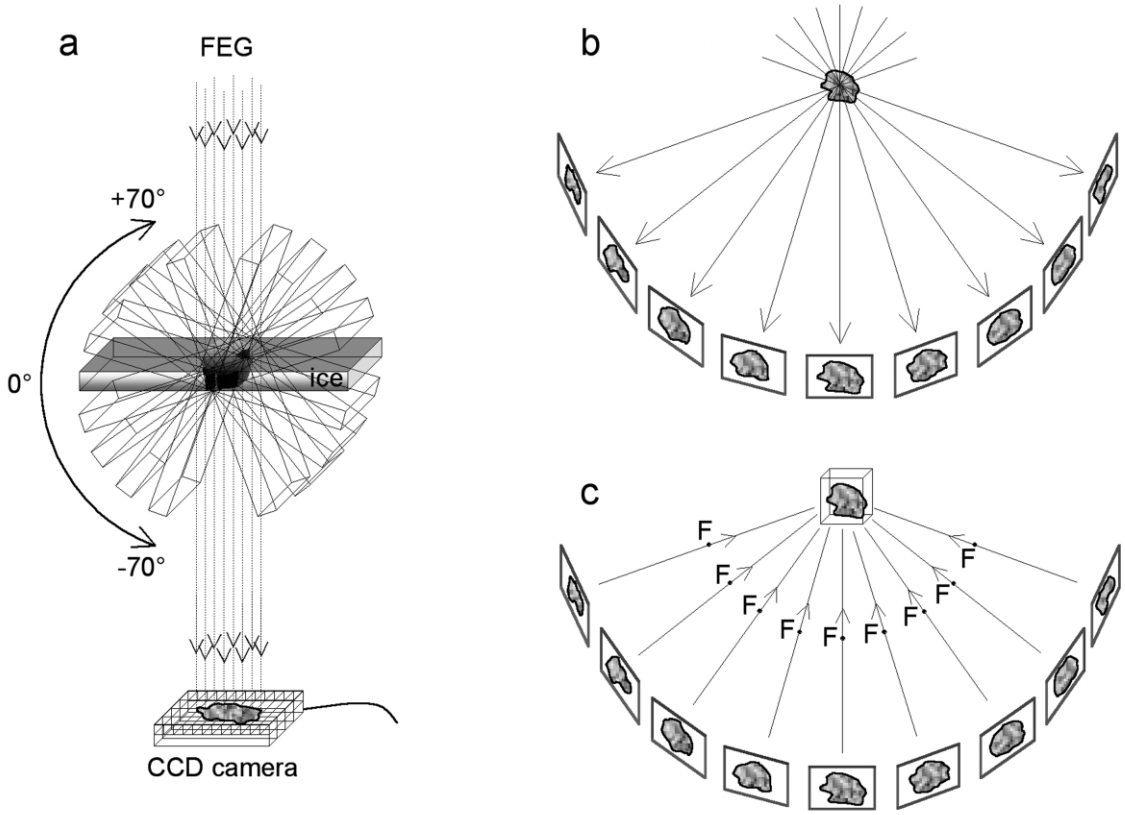

Fig. 1. Principle of electron tomography. The basic idea underlying this method is to record series of 2D transmission electron micrographs (projection images) at different tilt angles for individual 3D objects. In practice (a), the specimen holder is tilted incrementally around an axis perpendicular to the electron beam (preferentially supplied by a field emission gun—FEG), and projection images of the same specimen area are recorded on a CCD camera at each position. Tilt increments are typically 1.5–5° and the tilt range is approximately $\pm 70°$. A more schematic diagram (b) illustrates the images projected by a specimen at successive tilt angles. After mutual aligning all of these projection images, they are synthesized into a density map (the tomogram) by a 'weighted backprojection' [21] procedure (c), effected in Fourier space. This map represents the distribution of density through the specimen volume.

embedding in amorphous ice as a result of rapid freezing [5]. Although stained plastic sections from conventional embeddings have enhanced contrast and greater stability in the electron beam than vitrified whole mounts or cryosections, they suffer from the traditional concerns about artifacts induced by fixation and drying.

The most widely practiced method of vitrifying is plunge-freezing. A drop of buffer containing the specimen and colloidal gold, included to provide alignment markers, is applied to a grid, excess fluid is blotted away, and the sample is plunged into liquid ethane. The grid is then stored in liquid nitrogen until it is transferred into a pre-cooled EM cryoholder for observation. Another vitrification technique, high-pressure freezing, is the method of choice for thicker specimens destined for cryosectioning because it can achieve vitrification to a depth of ~ 300 μm [22,23]. However, despite recent progress [24–26], the preparation and handling of vitrified sections remains distinctly challenging.

2.2. Instrumentation and data acquisition

Tomographic data are typically acquired using a computer-controlled electron microscope equipped

with an eucentric goniometer. For vitrified specimens, the microscope has to be operated under low-dose conditions, searching for areas of interest at low magnification, and focussing on areas adjacent to those that will actually be recorded. Data are recorded digitally on CCD (charge-coupled device) cameras. Commercially available models vary in pixel size, scintillator performance, and array size (up to 4×4 K pixels) [27,28]. The use of an energy filter to remove inelastically scattered electrons can significantly improve image contrast and resolution, especially for thicker specimens [29,30]. A key milestone in the development of electron tomography has been the maturing of automated procedures capable of sequential recording of 80–120 or so projections covering angular ranges of up to $+/-70°$, throughout which the specimen is kept centered, a uniform level of focus is maintained, and the cumulative electron dose is kept within tolerable limits [31–34].

The successful application of cryotomography relies on the principle of dose fractionation: i.e. to a first approximation, the specimen sustains the same amount of damage from a given quota of imaging electrons, whether applied in a single exposure or partitioned over a tilt series [35–37]. In consequence, an end-product density map may be reliable to a certain resolution and SNR (see below) although it is computed from prohibitively noisy projections. The necessary electron dose for depicting features at $\sim$4 nm resolution is 40–100 $e^-/Å^2$ (4000–10000 e^-/nm^2) [13,36,37], close to the total maximal tolerable dose for vitrified specimens maintained at liquid–nitrogen temperature of $\sim$50 $e^-/Å^2$ [38].

2.3. Reconstruction into tomograms

A typical tilt series might contain 71 projections, covering the range of $+/-70°$ in 2° increments. Although the data acquisition protocol keeps the specimen approximately centered, the recorded projections must first be mutually aligned to establish a common coordinate system. Alignment methods currently used fall in two main classes, those based on fiducial markers [39], and those based on correlation functions [40,41]. Most protocols use a combination of both techniques. In either case, gold particles of 10 nm or so in diameter play a crucial role as alignment markers. Since they scatter electrons strongly, they are detectable even in low-dose, low-contrast, cryomicrographs. In alignment by cross-correlation, several strategies are possible: for instance, successive projections may be aligned with each other since they should resemble each other quite closely, the rotation between them being small. Alternatively, in an iterative calculation, each projection can be aligned with a reprojection of the current reconstruction; or the calculation of correlations can be restricted to areas around gold particles where the SNR is relatively high. Reconstruction typically involves back-projecting each projection across the volume [42], after applying appropriate weighting functions to the projections [43]. The result of the reconstruction is a 3D volume of digital data—the tomogram. All steps required to complete this analysis have been implemented in software packages like EM [44] and IMOD [45].

2.4. Interpreting cellular tomograms: recognizing macromolecular complexes

Tomograms contain imposing quantities of information. With 1 nm sampling, a tomogram of dimensions $1024\times1024\times1024$ covers a cubic micron of cellular space in 10^9 voxels. In practice, only half of this volume (in the z-dimension, along the optical axis) may be usable, but the complexity of this subvolume is still high, it is densely populated, and—despite optimized experimental technique—the tomogram will inevitably be contaminated with noise. Interpretation of such data sets is a much different proposition from, say, interpreting a density map from crystallography or cryo-EM. State-of-the art cellular tomograms from specimens of 150–200 nm thickness attain a resolution of approximately 5–8 nm but the level of residual noise is substantial, despite filtering (see below). Nevertheless, one may expect to pick out large-scale structures like cytoskeletal filaments or membranes, relying on continuity of density in one or two dimensions, respectively [46,47]. However, these components occupy only a small fraction of the total volume and the rest of the tomogram has still to be interpreted—from a view-

point whose priorities will vary with the observer. This challenging proposition, which attracts much active research [48], requires a combination of interactive three-dimensional graphics and automated data-sifting using pattern recognition techniques, assisted in both cases by computational procedures for noise reduction and image segmentation [49–51].

Given the uniqueness of each cellular tomogram, the prospects for noise reduction are quite limited compared to single-particle analysis which benefits greatly from averaging. If there is reason to suppose that resolution does not extend past a certain limit, say 5 nm, the tomogram may be band-limited at that point, eliminating high-frequency noise. More sophisticated 'de-noising' procedures, based on the same general principle but employing 'diffusion' criteria based on local continuity of density have been developed [52,53]. Although the net improvement in SNR from such methods can never be large, they have been demonstrated to substantially enhance the interpretability of cryotomograms.

One promising approach to interpretation involves automated searching through the experimental volume for copies of a known complex by cross-correlation techniques. As search template, a representation of the complex of interest obtained by single-particle cryo-EM or X-ray crystallography is required. Such templates should have higher resolution than the tomogram and be comparatively noise-free. Machine-based identification of complexes via such structural signatures is superior to visual inspection in objectivity and reproducibility but presents a formidable computational challenge in view of the three-dimensional nature of the correlation function, the large size of the search volume, the a priori unknown orientations of the intracellular complexes relative to the template, and the fact that a separate search has to be mounted for each complex. Nevertheless, in recent model experiments with in vitro mixtures of three bacterial complexes of comparable size and shape—the 20S proteasome, the thermosome, and GroEL—a success rate of over 90% in identifying the respective complexes was achieved at a SNR typical for energy-filtered tomographic data [50]. Although discrimination will be more difficult in densely crowded intracellular milieus (the congestion of complexes in these specimens was much lower than is typically encountered in vivo—see below), this represents encouraging progress.

2.5. Resolution and signal-to-noise ratio

In electron microscopy, resolution and SNR are closely linked. Although a weak signal may persist in a micrograph to high resolution, in practice, usable resolution will be limited to the spatial frequency to which an acceptable SNR is maintained [17,54]. This fact of optical life holds particularly true for tomography, where residual noise is an important issue. Apart from noise, there are also sampling-related considerations that bear on the resolution of tomograms. Two of them have to do with the coverage of the angular range: How finely and how completely is it covered?

The resolution (d) of a reconstruction of an object of diameter D from N equally spaced, noise-free, projections covering the full angular range is limited to $d \sim \pi\ \mathrm{D}/\mathrm{N}$ [55]. Applying this formula to a tomographic specimen 200 nm thick, sampled at angular increments of 1.5°, the resolution is theoretically limited to $\sim$5 nm. However, due to physical constraints, the full angular range cannot be accessed but is restricted to approximately $\pm 70°$. Considered in Fourier space, this results in a 'missing wedge' of data, whose absence results in anisotropic resolution; i.e. the resolution in the z-dimension is approximately 50% lower [56]. In our example, the resolution falls to $\sim$7 nm in this direction.

Tomograms, especially cryotomograms, suffer from generally low SNRs [37,46]. The noise derives from several sources. Because the projections are recorded at very low dose, there are statistical fluctuations referred to as 'shot noise'. Noise also stems from incipient radiation damage, progressively so towards the end of the tilt series [38]. Additionally, noise can enter during the calculation of the tomogram from imperfect alignment of projections; non-uniform focus over the tilt series; and increased specimen thickness at high tilt, giving rise to more multiple scattering events. Zero-loss energy filtering, i.e. removal of inelastically scattered electrons, improves image

contrast by minimizing the loss of resolution and contrast from chromatic aberration [29,30]. This is of particular importance when investigating biological specimens with a thickness of about or larger than the mean free path length of electrons (~200 nm in vitreous ice at an acceleration voltage of 120 kV).

In biological EM generally, one cannot be sure that theoretically expected resolutions are being attained and it is normal practice to apply empirical measures of resolution to the experimental data. In single-particle analysis, several measures based on consistency within a data set are used, such as the differential phase residual [15], Fourier ring correlation [16], and spectral signal-to-noise ratio [17]. For tomograms, such measures are not practicable and the issue of valid resolution criteria is still an area of active research [48]. Ideally, one might be able to distinguish a feature of known spacing: for instance, microtubules have a characteristic axial spacing at 4 nm, and actin filaments, at ~5.5 nm. More generally, if a complex of interest can be identified in the tomogram for which a reference structure (at relatively high resolution) is available, quantitative comparison between them can provide a measure of resolution, in terms of the frequency limit beyond which the correlation between the tomogram and the reference structure falls below an acceptable threshold. If such complexes are not detectable in the tomogram, they could be added to the specimen to serve as a resolution sensor.

2.6. Prospects for future progress

In principle, resolution could be improved by increasing the number of projections and the noise level could be reduced by working with higher electron doses. However, the resulting increase in radiation damage to vitrified specimens may be counterproductive. In this context, the prospect of working with liquid–helium-cooled specimen holders at 4–10 K rather than liquid–nitrogen-cooled specimens (~90 °K) appears to offer a significant increase in radiation-hardiness, by a factor of three or more [4]. A second possibility is to reduce the 'missing wedge' to a 'missing pyramid' by use of double-tilt holders [57,58]. This innovation should reduce the falloff in resolution in the dimension along the optical axis. There also appears to be scope for further improvements in computational aspects of tomography, including more accurate alignment of projections and more powerful segmentation algorithms.

3. Cryotomography of single cells: prokaryotes and eukaryotes

The relatively small size of many prokaryotes (~1 μm) allows them to be examined in toto by cryotomography after rapid quenching leaves the cells embedded in a thin layer of amorphous ice. It is not even necessary to remove the culture medium prior to freezing. For such specimens, cryotomography has the additional advantage of being fast compared to conventional thin sectioning which involves lengthy protocols of chemical fixation followed by dehydration and plastic embedding, or of freeze-substitution in which (cryo)fixation is fast but subsequent steps are slow. Tilt series are recorded within a few hours by (largely) automated procedures and shortly thereafter, the reconstructed tomograms are available for inspection; they may be sectioned optically in all desired directions by the observer and segmented for visualization. Cryotomograms convey the natural density distribution inside cellular volumes, unlike conventional thin sections which afford representations convoluted by staining reactions that produce intricate mixtures of positive and negative staining, compromizing interpretation in molecular terms.

To illustrate cryotomography of prokaryotes as currently practised, single planes (equivalent to Section 1 nm thick) are shown of the archaeon *Thermoproteus tenax* in Fig. 2a, and of the bacterium *Thermotoga maritima* in Fig. 2b. It is evident from these images that the cytoplasms of both cells are densely packed, in keeping with the scenario depicted in Goodsell's cartoons [http://www.scripps.edu/pub/goodsell/], with molecules literally touching each other. It is noteworthy, however, that the periplasmic space of *Thermotoga* cell is less densely populated than its cytoplasm (Fig. 2b). The most striking aspect of the *Ther-*

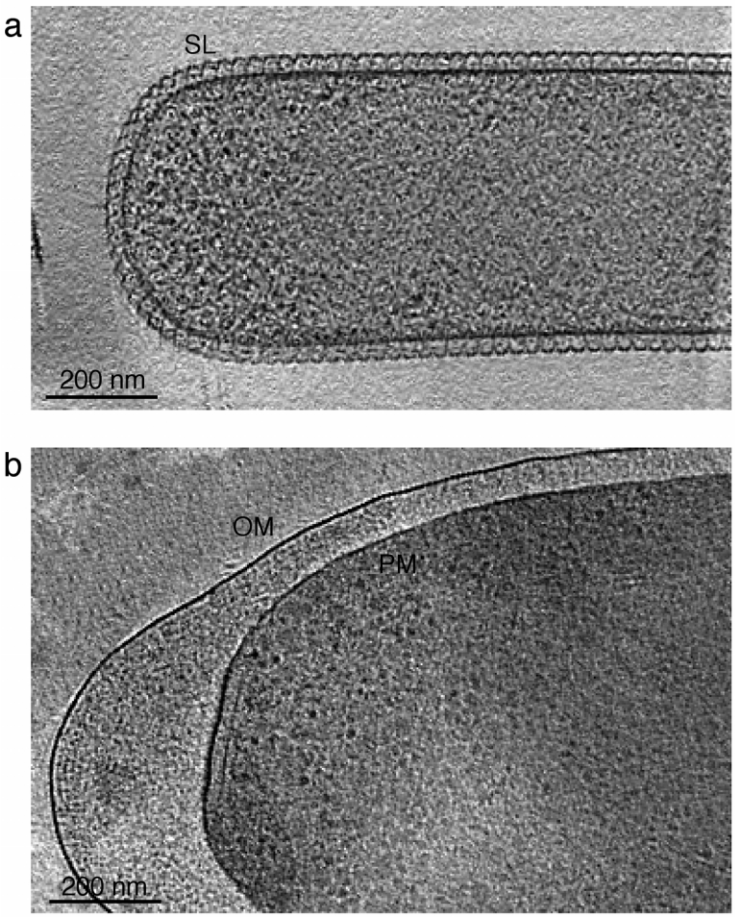

Fig. 2. Cryotomography of prokaryotes. Suspensions of whole cells in growth medium were vitrified by plunge-freezing (no chemical fixation or staining was applied), and tomographic data sets were recorded under low-dose conditions: the cumulative electron dose was between 30 and 50 $e^{-}/Å^{2}$). Following 3-D reconstruction, *x*;*y* slices (perpendicular to the optical axis) were extracted from the tomogram for display. (a) shows such a slice through the archaeon *Thermoproteus tenax* and (b) one through the bacterium *Thermotoga maritima*. The *Thermoproteus* cell is covered by a protein surface layer (SL) which is anchored to the underlying plasma membrane [59]; jointly they delimit an extracytoplasmic space analogous to the periplasmic space of bacteria. *Thermotoga maritima* possesses an outer membrane (OM) which is linked to the plasma membrane (PM) by a filiform spacer protein (Ompα) over most of the cell body except for the pole regions [90]. Obviously, in both organisms the periplasmic space is more dense than the surrounding medium, but much less densely packed with macromolecules than the crowded cytoplasm. Given the residual noise and the crowding, segmentation into individual macromolecules is, for the most part, not possible. However, sophisticated pattern recognition techniques should make it possible to detect large, morphologically distinctive, macromolecular complexes in tomograms, and thus map their intracellular distributions.

moproteus cell is its elaborate surrounding S-layer of protein [59] (Fig. 2a).

The larger dimensions and greater fragility of most eukaryotic cells complicate the prospects for preparation by direct vitrification and comparably detailed visualization. Without cryoprotectants, vitrification can only be achieved in specimens a few microns thick [5], and increased thickness imposes a proportionally greater demand on the number of projections required to reconstruct the experimental volume to the currently targeted resolution of 5–8 nm (see above). However, some cultured cells are

quite flat (i.e. <1 μm thick) and should be eligible for cryotomography without changing the protocols for specimen preparation or data collection.

A cryotomogram of a cell of the slime mould *Dictyostelium discoideum* is shown in Fig. 3. It is apparent that its cytoplasm is less crowded than in the prokaryotes shown in Fig. 2. This property facilitates the segmentation of structural features for further analysis. The actin cytoskeleton is clearly visible even in the'raw' tomograms (i.e. without denoising). This property makes it possible to analyze, at the level of individual filaments, modes of interactions between filaments (branching, crosslinks) or between filaments and the plasma membrane [60].

4. Macromolecular crowding inside cells

All cells are densely populated with macromolecules. Their dense packing—crowding—has functional repercussions at several levels: for example, in regulating activity [61], in placing a premium on motor-propelled transport over diffusion-based transport [62], and in affecting the propensity of constituents to polymerize or aggregate. Crowding also has practical implications for the interpretation of tomograms. For a given resolution and SNR, the lower the packing density (crowding), the better the chances that a free-standing complex will be rendered as such instead of as part of an amalgum in which it is artifactually fused with neighboring molecules.

4.1. Concepts

Cells are not simply bags containing freely diffusing and randomly colliding macromolecules. Rather, they have a well defined, if stochastically variable, organization that includes compartmentation within membrane-bound organelles (closed compartments) and in multicomponent complexes (open compartments). An excellent account of the physical properties of the cytoplasm and cytoarchitecture was recently compiled by Luby-Phelbs [63]. Recently, microrheology experiments identified cells as soft glassy material existing close to the glass transition rather than fluid-like and undergoing gel–sol transitions [64].

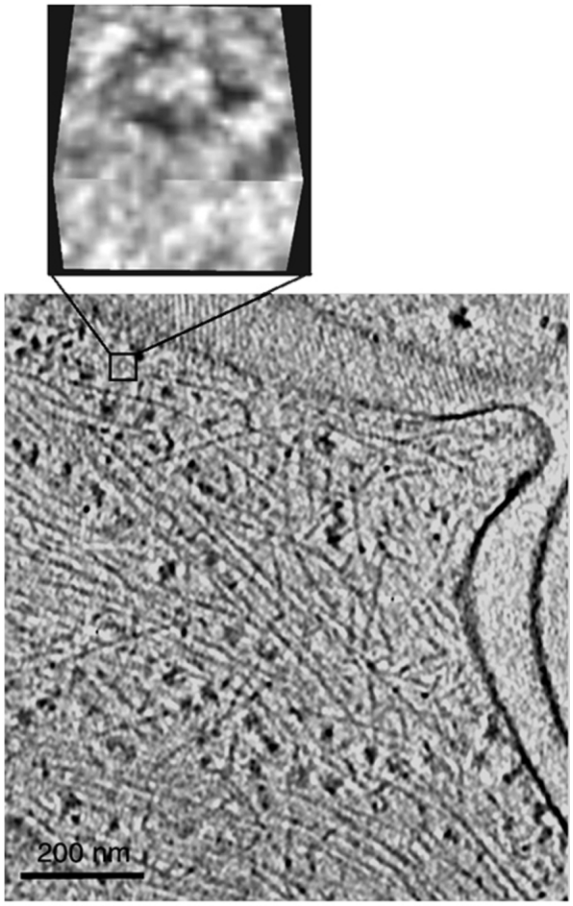

Fig. 3. Cryotomography of eukaryotes. A section through a tomogram of a frozen-hydrated *Dictyostelium* cell grown directly on an EM grid coated with a carbon film is shown in (a). The actin cytoskeleton is clearly visible. With such data sets, it is possible to study features of the actin network with a non-invasive method at unprecedented resolution. Interspersed in the actin network is a variety of particles, most of them unidentified. The larger, rather dense, particles probably represent ribosomes. Since the cytosol is not too crowded, it is possible to cut out in silico subtomograms (top) around the particles and to subject them to further analysis (see Fig. 4).

Macromolecules have evolved to function in crowded, heterogeneously populated, environments [65,66]. They occupy 20–30% of the total cellular volume, and this subvolume is sterically inacces-

Table 1
Relative translational diffusion coefficients (D/D_0) for different cell compartments[a]

Diffusing molecule	Investigation system	Cytoplasm	Nucleus	Mitochondria	ER[b]	Reference
FITC-dextran and FITC-ficoll	MDCK epithelial cells and swiss 3T3 fibroblasts	0.26 0.27	0.25 0.27			[80]
BCEC-fluorescein	Swiss 3T3 fibroblasts	0.27				[78]
DNA-fluorescein (100 bp)	HeLa cells	0.19	≈0			[85]
GFP	CHO-K1 mammalian epithelial cells	0.31				[79]
GFP	Fibroblast, liver, muscle, epithelial cell lines			0.23–0.34		[82]
GFP	CHO-K1 mammalian epithelial cells				0.06–0.11	[83]
GFP	*Dictyostelium discoideum* actin network disrupted	0.27 0.48	0.25			[81]
GFP	*Escherichia coli*	0.09				[77]

[a] Relative to water; adapted from [64].
[b] Endoplasmatic reticulum.

sible to other molecules. This excluded volume effect, known as 'macromolecular crowding', has dramatic—and often underappreciated—consequences [67].

In the first place, the effective concentrations of molecules are higher than their nominal values would suggest, and this amplification promotes high efficiency in metabolic pathways [68]. Second, diffusion rates are reduced (see below). Sheer proximity results in numerous short-lived non-specific associations that impinge on the rates and equilibria of specific interactions [61]. In the context of protein assembly/disassembly, crowding is expected to stabilize native structures and to enhance folding and oligomerization of macromolecules to form functional complexes [63,69]. Non-specific aggregation and misfolding are also promoted by crowding and have to be countered by molecular chaperones [65,69].

4.2. Quantification of macromolecular crowding

The first measurements involved estimating intracellular concentrations of macromolecules. For example, for *E. coli*, the total concentration of nucleic acids and protein was estimated at 300–400 g l^{-1}, occupying 25–33% of the volume and constituting > 90% of the dry weight [70,71]. Later, methods based on quantifying intracellular diffusion were developed. Translational diffusion coefficients of small metabolites and of water have been determined in various compartments by NMR techniques [72]. With the advent of fluorescent probes, in particular, green fluorescent protein (GFP), direct observation of molecular movements inside cells became possible [73]. The most commonly applied method of studying translational diffusion is Fluorescent Recovery After Photobleaching (FRAP) [74–76], in which an apparent diffusion coefficient is determined from the kinetics of return of unbleached tracer molecules into an area from which fluorescing tracers have been purged by photobleaching with a focussed laser beam. The method has been applied to the cytoplasms of both prokaryotic [77] and eukaryotic cells [78,79], the nucleus [80,81], mitochondria [82], and the endoplasmatic reticulum [83]. The parameter measured is the apparent translational diffusion coefficient D/D_0 relative to that in water, or its reciprocal, representing cellular viscosity. Table 1 lists diffusion coefficients for different compartments and organisms. It should kept in mind that, beside crowding, macromolecular mobility is likely to be affected by other factors, such as binding to cytoskeletal structures [65,84] as exemplified by the doubled diffusion coefficient observed in *Dictyostelium discoideum* cells after disruption of the actin network with lantruculin-A [81], Table 1].

4.3. Comparison of different compartments

Because of their small size, it is only recently that bacteria have become accessible to improved FRAP techniques [77]. From Table 1, it is clear that the bacterial cytoplasm is significantly more viscous than the eukaryotic cytoplasm. Binding of diffusand to the cytoskeleton cannot be the reason for this distinction as such networks are mainly absent in bacteria; however, binding to other relatively immobile structures (e.g. the nucleoid) is not ruled out. The data can explain measured response times in bacteria on the basis of mediator protein diffusion [77]. Thus, higher crowding in bacterial cells compared to eukaryotic ones seems to be the case.

The available data on cytoplasm viscosity in eukaryotic cells are consistently 3–4 times higher than in water. Surprisingly, mitochondria do not differ markedly from cytoplasm as one might suspect from the endosymbiont origin of this organelle. The nucleus is only slightly more viscous than the cytoplasm, although the observed near-immobility of DNA fragments [85] indicated that all molecules do not experience the same effective viscosity. Diffusion of GFP in the aqueous lumen of the endoplasmic reticulum was found to be 3–6 times slower than in cytoplasm. Possibly, this retardation may be due in part to the characteristic topology of this compartment allowing GFP to diffuse back into the bleached region only via the tubular conduits.

Generally, the measured values give a mean viscosity value and inhomogenities in the compartments are likely. A cytoplasmic microdifferentiation into (i) an actin filament-rich part excluding organelles and even particles, and (ii) a microtubule-rich organelle-containing part has been shown by steric exclusion of large fluorescent tracer particles [86].

Recently cryotomographic analysis of *D. discoideum* cells grown on carbon-coated EM grids has detected a markedly less crowded cytoplasm than in prokaryotes [60]. This observation is fully consistent with the foregoing diffusion-based studies (Table 1). In this context, cryotomography could, in fact, be used to obtain a quantitative measure of the crowding in all cellular compartments, provided that suitable calibration standards are used to set a threshold density for rendering the tomograms.

5. Implications and prospects for complex biology

5.1. Identification and mapping of known complexes

The prospect of being able to identify complexes in situ raises intriguing possibilities in a cell biological context. First, the distribution of each complex within a cell may be mapped (‘molecular demographics’). Such distributions—which are expected to vary stochastically between ostensibly identical cells—may already be addressed by immuno-labelling EM [87]. Cryotomography offers an independent approach that is not contingent on epitope accessibility. Moreover, variations between cell types, or between nutritional states of a given cell type, or according to the phase of the cell cycle, or in response to external stimuli such as heat-shock or drug treatment, or resulting from specific mutations, may be systematically studied and compared. Second, having localized the complexes, one may extract the corresponding set of subtomograms; fractionate them by multivariate statistical analysis; and average them within each supposedly homogeneous subfamily. In this way, one may hope to visualize—at an improved SNR—functionally differentiated variants of the same basic complex.

Realization of these exciting prospects will depend critically on the quality of the tomograms. In techniques that identify complexes as local maxima of a correlation function, the question arises of how to determine a threshold for which cross-correlation coefficients should be considered significant. This question is complicated by the fact that correlation coefficients of comparable significance may vary markedly in numerical value according to the intrinsic structure of the complex (e.g. [88]). Here, a priori knowledge of the likely cellular complement can be useful: if there are $\sim N$ copies per cell, one should focus on the N correlation maxima with the highest coefficients. Nevertheless, any strategy for mapping protein

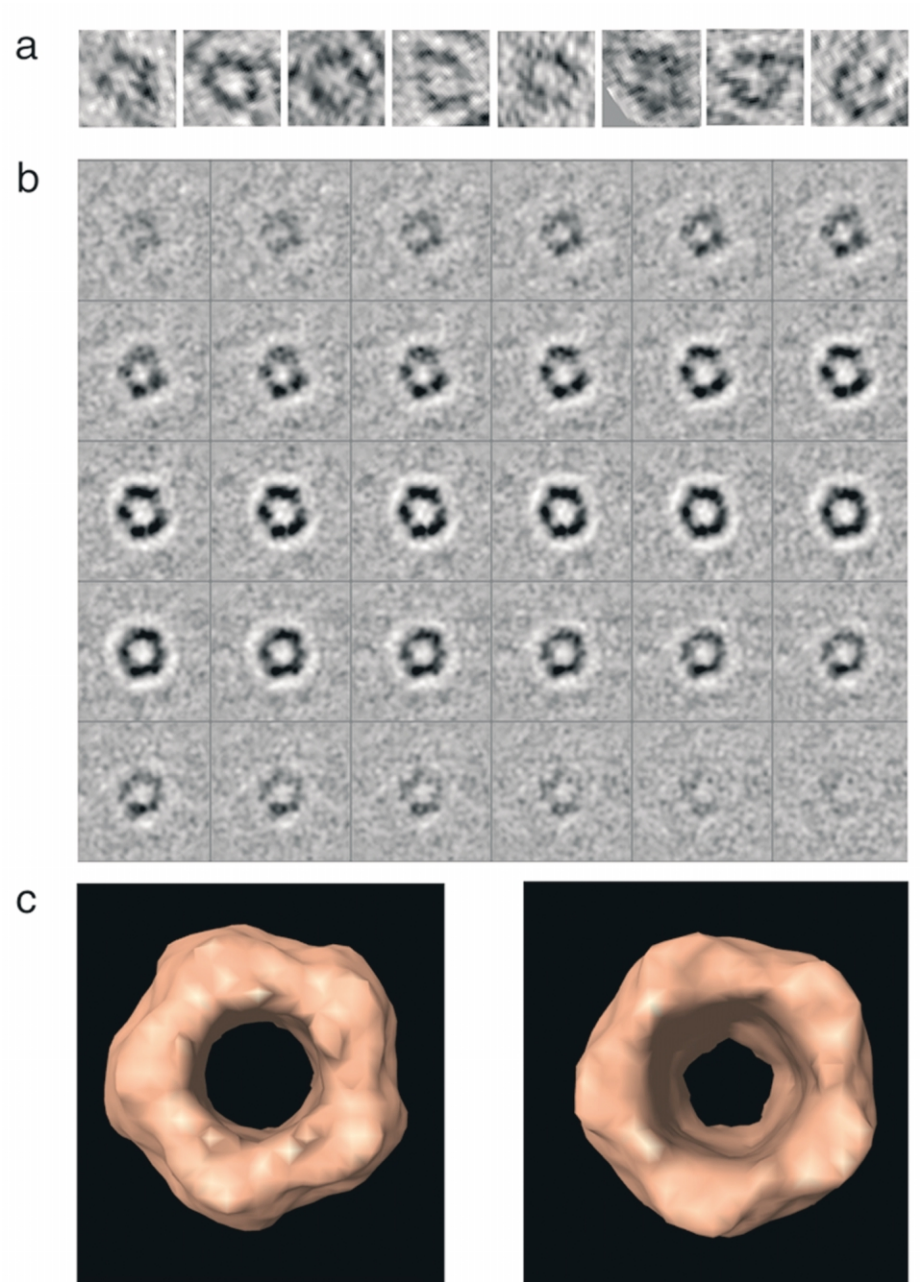

Fig. 4. Detection of a novel particle in cryotomograms of *Dictyostelium* cells. Abundant in these tomograms are cup-shaped particles with a diameter of ~ 20 nm. One such particle is contained in the area blown up in Fig. 3. Subtomograms containing such particles were cut out interactively and aligned in three dimensions. Symmetry analysis by ROTASTAT [91] detected only five-fold symmetry as statistically significant. The subtomograms were classified and averaged, revealing a pentameric complex. (a) Gallery of projections of subtomograms; (b) *x*;*y* slices through the 3-D averaged particle; (c) surface-rendered representation of the averaged particle viewed up and down the *z*-axis.

complexes in tomograms must take the crowding into account.

5.2. Detection of novel complexes inside cells

Although the number of macromolecular complexes implicated in a wide range of cellular functions is growing rapidly [18–20], it seems inevitable that many more remain to be discovered. The complexes currently on record tend to be those that are relatively abundant and stable, and there are surely many more that are sparse or transient or too fragile to survive the isolation procedures in current use. In this context, cryotomography offers the possibility to identify morphologically distinctive complexes in situ. An example is shown in Fig. 4 of a 5-fold-symmetric cup-shaped particle, approximately 20 nm in diameter, which we have observed in tomograms of the cytoplasm of *Distyostelium* cells [60], aided by their relatively low crowding. To our knowledge, this particle does not correspond to any previously described structure.

Such observations can form the basis for isolation and subsequent biochemical characterization of novel complexes. At each stage, EM and tomography may be used to identify the fractions containing the complex of interest and to assess its state of preservation. In this approach, the traditional pathway of discovery leading from biochemistry to structural analysis is reversed as in the case of the thermosome which was originally detected by EM of cell lysates and then purified, using micrographs to assay the purification steps [89].

5.3. Conclusions

Hitherto, almost all cellular cryotomographic studies have been confined to prokaryotes. It is now apparent that relatively flat eukaryotic cells such as *D. discoideum* are equally accessible to this approach, with the added bonus that eukaryotic cells appear to be more amenable than prokaryotic cells to the identification of macromolecules *in situ* on account of their markedly lower degree of crowding. Other eukaryotic specimens that could immediately be studied in this way include amoebae or neurons that, in places, are thin enough to allow high resolution cryotomography without recourse to sectioning.

At a resolution of ~5 nm, the reconstructed volume of a whole cell contains an enormous amount of information. It affords a 3-D picture that contains the overall structure of organelles, subcompartments, and the cytoskeleton inside the environment of an intact cell as well as its entire proteome and, in principle, should allow a complete description of its spatial organization. For 'mining' of these data sets to ensure full exploitation of their information content, new strategies and innovative image analysis techniques are needed. As noted above, new modes of image acquisition will make resolution more isotropic and 'denoising' of tomograms will help to combat the residual noise which currently obscures much of the information present.

Acknowledgments

We thank Dr Irina Gutsche for help with tomogram alignment and Dr Eva Kocsis for performing a symmetry detection analysis. This work was supported in part by Fellowships from the Alexander von Humboldt Stiftung (to A.C.S.), the Deutsche Forschungsgemeinschaft and the Max-Planck-Society (to K.G.), and the European Commission Marie Curie Individual Fellowship (to O.M.).

References

[1] W. Chiu, A. McGough, M.B. Sherman, M.F. Schmid, High-resolution electron cryomicroscopy of macromolecular assemblies, Trends Cell Biol. 9 (1999) 154–159.
[2] R.M. Glaeser, Review: Electron crystallography: Present excitement, a nod to the past, anticipating the future, J. Struct. Biol. 128 (1999) 3–14.
[3] W. Baumeister, A.C. Steven, Macromolecular electron microscopy in the era of structural genomics, Trends Biochem. Sci. 25 (2000) 624–631.
[4] V.M. Unger, Electron cryomicroscopy methods, Curr. Opin. Struct. Biol. 11 (2001) 548–554.
[5] J. Dubochet, M. Adrian, J.J. Chang, et al., Cryo-electron microscopy of vitrified specimens, Q. Rev. Biophys. 21 (1988) 129–228.
[6] T. Walz, N. Grigorieff, Electron crystallography of two-dimensional crystals of membrane proteins, J. Struct. Biol. 121 (1998) 142–161.

[7] H.R. Saibil, Macromolecular structure determination by cryo-electron microscopy, Acta Crystallogr. Sect. D-Biol. Crystallogr. 56 (2000) 1215–1222.
[8] J. Ruprecht, J. Nield, Determining the structure of biological macromolecules by transmission electron microscopy, single particle analysis and 3D reconstruction, Prog. Biophys. Mol. Biol. 75 (2001) 121–164.
[9] A.J. Koster, R. Grimm, D. Typke, et al., Perspectives of molecular and cellular electron tomography, J. Struct. Biol. 120 (1997) 276–308.
[10] W. Baumeister, R. Grimm, J. Walz, Electron tomography of molecules and cells, Trends Cell Biol. 9 (1999) 81–85.
[11] B.F. McEwen, M. Marko, The emergence of electron tomography as an important tool for investigating cellular ultrastructure, J. Histochem. Cytochem. 49 (2001) 553–563.
[12] D. Nicastro, A.S. Frangakis, D. Typke, W. Baumeister, Cryo-electron tomography of Neurospora mitochondria, J. Struct. Biol. 129 (2000) 48–56.
[13] R. Grimm, H. Singh, R. Rachel, D. Typke, W. Zillig, W. Baumeister, Electron tomography of ice-embedded prokaryotic cells, Biophys. J. 74 (1998) 1031–1042.
[14] J.R. McIntosh, Electron microscopy of cells: A new beginning for a new century, J. Cell Biol. 153 (2001) F25–F32.
[15] J. Frank, A. Verschoor, M. Boublik, Computer averaging of electron-micrographs of 40S ribosomal-subunits, Science 214 (1981) 1353–1355.
[16] W.O. Saxton, W. Baumeister, The correlation averaging of a regularly arranged baterial-cell envelope protein, J. Microsc. Oxf. 127 (1982) 127–138.
[17] M. Unser, B.L. Trus, J. Frank, A.C. Steven, The spectral signal-to-noise ratio resolution criterion: computational efficiency and statistical precision, Ultramicroscopy 30 (1989) 429–433.
[18] B. Alberts, The cell as a collection of protein machines: Preparing the next generation of molecular biologists, Cell 92 (1998) 291–294.
[19] A.C. Gavin, M. Bosche, R. Krause, et al., Functional organization of the yeast proteome by systematic analysis of protein complexes, Nature 415 (2002) 141–147.
[20] Y. Ho, A. Gruhler, A. Heilbut, et al., Systematic identification of protein complexes in *Saccharomyces cerevisiae* by mass spectrometry, Nature 415 (2002) 180–183.
[21] M. Radermacher, in: J. Frank (Ed.), Weighted back-projection methods, in: Electron tomography, three-dimensional imaging with the transmission electron microscope, Plenum Press, New York, 1992, pp. 91–116.
[22] E. Shimoni, M. Müller, On optimizing high-pressure freezing: from heat transfer theory to a new microbiopsy device, J. Microsc. Oxf. 192 (1998) 236–247.
[23] D. Studer, W. Graber, A. Al-Amoudi, P. Eggli, A new approach for cryofixation by high-pressure freezing, J. Microsc. Oxf. 203 (2001) 285–294.
[24] N.S. Blanc, D. Studer, K. Ruhl, J. Dubochet, Electron beam-induced changes in vitreous sections of biological samples, J. Microsc. Oxf. 192 (1998) 194–201.
[25] D. Studer, H. Gnaegi, Minimal compression of ultrathin sections with use of an oscillating diamond knife, J. Microsc. Oxf. 197 (2000) 94–100.
[26] J. Dubochet, N.S. Blanc, The cell in absence of aggregation artifacts, Micron 32 (2001) 91–99.
[27] I. Daberkow, K.H. Herrmann, L. Liu, W.D. Rau, H. Tietz, Development and performance of a fast fibre-plate coupled CCD camera at medium energy and image processing system for electron holography, Ultramicroscopy 64 (1996) 35–48.
[28] A.R. Faruqi, S. Subramaniam, CCD detectors in high-resolution biological electron microscopy, Q. Rev. Biophys. 33 (2000) 1–27.
[29] R. Grimm, A.J. Koster, U. Ziese, D. Typke, W. Baumeister, Zero-loss energy filtering under low-dose conditions using a post-column energy filter, J. Microsc. Oxf. 183 (1996) 60–68.
[30] R. Grimm, D. Typke, W. Baumeister, Improving image quality by zero-loss energy filtering: quantitative assessment by means of image cross-correlation, J. Microsc. Oxf. 190 (1998) 339–349.
[31] D. Typke, K. Dierksen, W. Baumeister, Automatic electron tomography, Proc. 49th Ann. Mtg. of the Electron Microscopy Society of America, San Francisco Press, San Francisco, 1991, pp. 544–545.
[32] K. Dierksen, D. Typke, R. Hegerl, A.J. Koster, W. Baumeister, Towards automatic electron tomography, Ultramicroscopy 40 (1992) 71–87.
[33] A.J. Koster, H. Chen, J.W. Sedat, D.A. Agard, Automated microscopy for electron tomography, Ultramicroscopy 46 (1992) 207–227.
[34] K. Dierksen, D. Typke, R. Hegerl, W. Baumeister, Towards automatic electron tomography. 2. Implementation of autofocus and low-dose precedures, Ultramicroscopy 49 (1993) 109–120.
[35] R. Hegerl, W. Hoppe, Influence of electron noise on 3-dimensional image-reconstruction, Z. Naturforsch. 31A (1976) 1717–1721.
[36] B.F. McEwen, K.H. Downing, R.M. Glaeser, The relevance of dose-fractionation in tomography of radiation-sensitive specimens, Ultramicroscopy 60 (1995) 357–373.
[37] B.E.H. Saxberg, W.O. Saxton, Quantum noise in 2D projections and 3D reconstructions, Ultramicroscopy 6 (1981) 85–90.
[38] J.F. Conway, B.L. Trus, F.P. Booy, W.W. Newcomb, J.C. Brown, A.C. Steven, The effects of radiation damage on the structure of frozen hydrated HSV-1 capsids, J. Struct. Biol. 111 (1993) 222–233.
[39] M.C. Lawrence, in: J. Frank (Ed.), Least-squares method of alignment using markers, in: Electron tomography, three-dimensional imaging with the transmission electron microscope, Plenum Press, New York, 1992, pp. 197–204.

[40] J. Frank, M. van Heel, Correspondence analysis of aligned images of biological particles, J. Mol Biol 161 (1982) 134–137.
[41] R. Guckenberger, Determination of a common origin in the micrographs of tilt series in 3-dimensional electron microscopy, Ultramicroscopy 9 (1982) 167–173.
[42] J. Frank, B.F. McEwen, in: J. Frank (Ed.), Alignment by cross-correlation, in: Electron tomography, three-dimensional imaging with the transmission electron microscope, Plenum Press, New York, 1992, pp. 205–214.
[43] J. Frank, M. Radermacher, T. Wagenknecht, A. Verschoor, A new method for three-dimensional reconstruction of single macromolecules using low-dose electron micrographs, Ann. N.Y. Acad. Sci. 483 (1986) 77–87.
[44] R. Hegerl, The EM program package: A platform for image processing in biological electron microscopy, J. Struct. Biol. 116 (1996) 30–34.
[45] J.R. Kremer, D.N. Mastronarde, J.R. McIntosh, Computer visualization of three-dimensional image data using IMOD, J. Struct. Biol. 116 (1996) 71–76.
[46] A. Stoschek, R. Hegerl, De-noising of electron tomographic reconstructions using multiscale transformations, J. Struct. Biol. 120 (1997) 257–265.
[47] A.S. Frangakis, R. Hegerl, Non-linear anisotropic diffusion in three-dimensional electron microscopy, Scale-Space Theories in Computer Vision 1682 (1999) 386–397.
[48] Proceedings of the Netherlands Academy Colloquium on Electron Tomography, Amsterdam, October 17-20, 2001. J. Struct. Biol. 138 (2002) part 1 and 2
[49] Y. Li, A. Leith, J. Frank, Tinkerbell: A tool for interactive segmentation of 3D data, J. Struct. Biol. 120 (1997) 266–275.
[50] J. Böhm, A.S. Frangakis, R. Hegerl, S. Nickell, D. Typke, W. Baumeister, Toward detecting and identifying macromolecules in a cellular context: Template matching applied to electron tomograms, Proc. Natl. Acad. Sci. USA 97 (2000) 14245–14250.
[51] A.S. Frangakis, R. Hegerl, Segmentation of two- and three- dimensional data from electron miscroscopy using eigenvector analysis, J. Struct. Biol. 138 (2002) 105–113.
[52] A.S. Frangakis, A. Stoschek, R. Hegerl, Wavelet transform filtering and non-linear anisotropic diffusion assessed for signal reconstruction performance on multidimensional biomedical data, IEEE Trans. Biomed. Eng. 48 (2001) 213–222.
[53] A.S. Frangakis, R. Hegerl, Noise reduction in electron tomographic reconstructions using non-linear anisotropic diffusion, J. Struct. Biol. 135 (2001) 239–250.
[54] R. Henderson, J.M. Baldwin, K.H. Downing, J. Lepault, F. Zemlin, Structure of purple membrane from Halobacterium halobium: Recording, measurement and evaluation of electron micrographs at 3.5 Å resolution, Ultramicroscopy 19 (1986) 147–178.
[55] R.A. Crowther, D.J. DeRosier, A. Klug, The reconstruction of a three-dimensional structure from its projections and its application to electron microscopy, Proc. Roy. Soc. London A 317 (1970) 319–340.
[56] J. Jimenez, A. Santisteban, J.-M. Carazo, J.L. Carrascosa, Computer graphic display method for visualizing 3-dimensional biological structure, Science 232 (1986) 1113–1115.
[57] P. Penczek, M. Marko, K. Buttle, J. Frank, Double-tilt electron tomography, Ultramicroscopy 60 (1995) 393–410.
[58] D.N. Mastronarde, Dual-axis tomography: An approach with alignment methods that preserve resolution, J. Struct. Biol. 120 (1997) 343–352.
[59] I. Wildhaber, W. Baumeister, The cell envelope of Thermoproteus tenax: Three-dimensional structure of the surface layer and its role in shape maintenance, EMBO J. 6 (1987) 1475–1980.
[60] O. Medalia, I.Weber, A.S. Frangakis, et al. Macromolecular architecture in eukaryotic cells visualized by cryo-electron tomography. Science (2002) in press.
[61] A.P. Minton, Molecular crowding: Analysis of effects of high concentrations of inert cosolutes on biochemical equilibria and rates in terms of volume exclusion, Meth. Enzymol. 295 (1998) 127–149.
[62] A.R. Reilein, S.L. Rogers, M.C. Tuma, V.I. Gelfand, Regulation of molecular motor proteins, Int. Rev. Cytol. 204 (2001) 179–238.
[63] K. Luby-Phelps, Cytoarchitecture and physical properties of cytoplasm: Volume, viscosity. diffusion, intracellular surface area, Int. Rev. Cytol. 192 (2000) 189–221.
[64] B. Fabry, G.N. Maksym, J.P. Butler, M. Glogauer, D. Navajas, J.J. Fredberg, Scaling the microrheology of living cells, Phys. Rev. Lett. 8714 (2001) 8102-1-4.
[65] R.J. Ellis, Macromolecular crowding: an important but neglected aspect of the intracellular environment, Curr. Opin. Struct. Biol. 11 (2001) 114–119.
[66] R.J. Ellis, Macromolecular crowding: obvious but underappreciated, Trends Biochem. Sci. 26 (2001) 597–604.
[67] A.P. Minton, Influence of excluded volume upon macromolecular structure and associations in 'crowded' media, Curr. Opin. Biotechnol. 8 (1997) 65–69.
[68] S.B. Zimmerman, A.P. Minton, Macromolecular crowding-biochemical, biophysical, and physiological consequences, Annu. Rev. Biophys. Biomolec. Struct. 22 (1993) 27–65.
[69] A.P. Minton, Implications of macromolecular crowding for protein assembly, Curr. Opin. Struct. Biol. 10 (2000) 34–39.
[70] S. Cayley, B.A. Lewis, H.J. Guttman, M.T. Record, Characterization of the cytoplasm of Escherichia coli K-12 as a function of external osmolarity-implications for protein-DNA interactions in vivo, J. Mol. Biol. 222 (1991) 281–300.
[71] S.B. Zimmerman, S.O. Trach, Estimation of macromolecule concentrations and excluded volume effects for

the cytoplasm of *Escherichia coli*, J. Mol. Biol. 222 (1991) 599–620.

[72] A.I. Garcia-Perez, E.A. Lopez-Beltran, P. Kluner, J. Luque, P. Ballesteros, S. Cerdan, Molecular crowding and viscosity as determinants of translational diffusion of metabolites in subcellular organelles, Arch. Biochem. Biophys. 362 (1999) 329–338.

[73] F.S. Wouters, P.J. Verveer, P.I.H. Bastiaens, Imaging biochemistry inside cells, Trends Cell Biol. 11 (2001) 203–211.

[74] D.E. Wolf, Designing, building, and using a fluorescence recovery after photobleaching instrument, Meth. Cell Biol. 30 (1989) 271–306.

[75] K. Luby-Phelps, Physical properties of cytoplasm, Curr. Opin. Cell Biol. 6 (1994) 3–9.

[76] A.S. Verkman, Green fluorescent protein as a probe to study intracellular solute diffusion, Meth. Enzymol. 302 (1999) 250–264.

[77] M.B. Elowitz, M.G. Surette, P.E. Wolf, J.B. Stock, S. Leibler, Protein mobility in the cytoplasm of *Escherichia coli*, J. Bacteriol. 181 (1999) 197–203.

[78] H.P. Kao, J.R. Abney, A.S. Verkman, Determinants of the translational mobility of a small solute in cell cytoplasm, J. Cell Biol. 120 (1993) 175–184.

[79] R. Swaminathan, C.P. Hoang, A.S. Verkman, Photobleaching recovery and anisotropy decay of green fluorescent protein GFP-S65T in solution and cells: Cytoplasmic viscosity probed by green fluorescent protein translational and rotational diffusion, Biophys. J. 72 (1997) 1900–1907.

[80] O. Seksek, J. Biwersi, A.S. Verkman, Translational diffusion of macromolecule-sized solutes in cytoplasm and nucleus, J. Cell Biol. 138 (1997) 131–142.

[81] E.O. Potma, W.P. de Boeij, L. Bosgraaf, J. Roelofs, P.J.M. van Haastert, D.A. Wiersma, Reduced protein diffusion rate by cytoskeleton in vegetative and polarized Dictyostelium cells, Biophys. J. 81 (2001) 2010–2019.

[82] A. Partikian, B. Olveczky, R. Swaminathan, Y.X. Li, A.S. Verkman, Rapid diffusion of green fluorescent protein in the mitochondrial matrix, J. Cell Biol. 140 (1998) 821–829.

[83] M.J. Dayel, E.F.Y. Hom, A.S. Verkman, Diffusion of green fluorescent protein in the aqueous-phase lumen of endoplasmic reticulum, Biophys. J. 76 (1999) 2843–2851.

[84] A.P. Minton, Confinement as a determinat of macromolecular structure and reactivity. 2. Effects of weakly attractive interactions between confined macrosolutes and confining structures, Biophys. J. 68 (1995) 1311–1322.

[85] G.L. Lukacs, P. Haggie, O. Seksek, D. Lechardeur, N. Freedman, A.S. Verkman, Size-dependent DNA mobility in cytoplasm and nucleus, J. Biol. Chem. 275 (2000) 1625–1629.

[86] D.W. Provance, A. McDowall, M. Marko, K. Luby-Phelps, Cytoarchitecture of size-excluding compartments in living cells, J. Cell Sci. 106 (1993) 565–578.

[87] P.J. Peters, W. Hunziker, Subcellular localization of Rab17 by cryo-immunogold electron microscopy in epithelial cells grown on polycarbonate filters, Meth. Enzymol. 329 (2001) 210–225.

[88] N. Cheng, B. Trus, D.M. Belnap, W.W. Newcomb, J.C. Brown, A.C. Steven, Handedness of *Herpes simplex* virus capsid and procapsid, J. Virol. 76 (2002) 7855–7859.

[89] B.M. Phipps, A. Hoffmann, K.O. Stetter, W. Baumeister, A novel ATPase complex selectivley accumulated upon heat shock is a major cellular component of thermiphilic archaebacteria, EMBO J. 10 (1991) 1711–1722.

[90] A.M. Engel, Z. Cejka, A. Lupas, F. Lottspeich, W. Baumeister, Isolation and cloning of Ompα, a coiled-coil protein spanning the periplasmic space of the ancestral eubacterium *Thermotoga maritima*, EMBO J. 11 (1992) 4369–4378.

[91] E. Kocsis, M.E. Cerritelli, B.L. Trus, N. Cheng, A.C. Steven, Improved methods for determination of rotational symmetries in macromolecules, Ultramicroscopy 60 (1995) 219–228.